IEEE Photonics Journal
An IEEE Photonics Society Publication

Open Access

Planar Plasmonic Terahertz Waveguide Based Upon One Dimensional Array of Pyramidal Corrugations and Refractive Index Sensing

Volume 12, Number 6, December 2020

KM Dhriti Maurya, *Member, IEEE*
Amir Ahmad
Gagan Kumar, *Senior Member, IEEE*

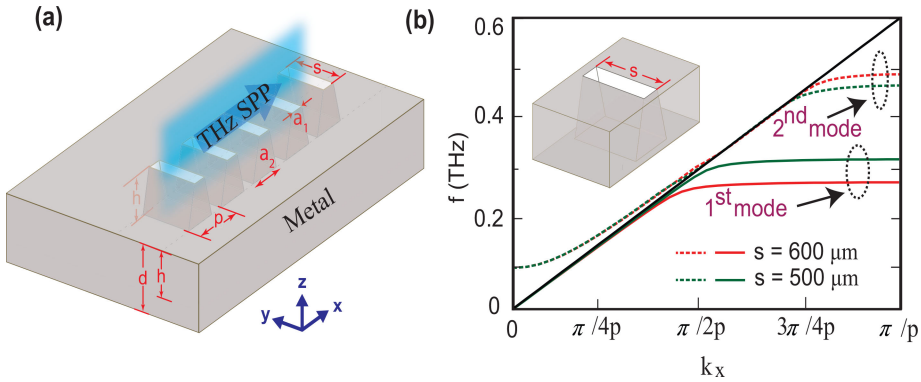

DOI: 10.1109/JPHOT.2020.3034549

Planar Plasmonic Terahertz Waveguide Based Upon One Dimensional Array of Pyramidal Corrugations and Refractive Index Sensing

KM Dhriti Maurya,[1] ***Member, IEEE***, **Amir Ahmad**,[2] **and Gagan Kumar**,[1] ***Senior Member, IEEE***

[1]Indian Institute of Technology Guwahati, Department of Physics, Guwahati 781039, India
[2]College of Information Technology, United Arab Emirates University, Al Ain 15551, UAE

DOI:10.1109/JPHOT.2020.3034549

Manuscript received October 2, 2020; revised October 19, 2020; accepted October 24, 2020. Date of publication October 28, 2020; date of current version December 2, 2020. This work was supported by the United Arab Emirates University start-up grant under Grant G00002668 and fund number 39031T101. Corresponding author: Amir Ahmad (e-mail: amirahmad@uaeu.ac.ae).

Abstract: We examine the refractive index sensor ability of the terahertz surface plasmon modes supported by a planar plasmonic terahertz (THz) waveguide. The waveguide is comprised of one-dimensional array of periodically arranged subwavelength scale pyramidal corrugations resulting in a plasmonic metamaterials waveguide. The waveguide exhibits strong field confinement along with the corrugated pattern. We have analyzed the dispersion property and quality factor of the fundamental as well as higher-order modes of the waveguide. In order to examine sensor capability, we used analytes of different refractive indices and observed a corresponding frequency shift. We further analyze the sensitivity of all the modes for the given volume of analyte and compare their sensing performance. We have employed the semi-analytical model to understand the numerical observations. The proposed waveguide approach can potentially result in highly sensitive refractive index sensors at terahertz frequencies.

Index Terms: Plasmonic, sensing, terahertz, waveguide.

1. Introduction

There has been considerable interest in exploring the sensing capability of terahertz electromagnetic waves in recent few years. The frequency of THz waves lies between microwave and mid-infrared regimes of the electromagnetic spectrum and exhibit nonionizing character because of their low energies [1]–[5]. This makes terahertz frequencies an ideal candidate for sensing several complex molecules whose rotational and vibrational modes fall in this frequency band [6]–[8]. In this context, several studies have been reported to sense biomolecules, proteins and chemicals whose spectral features lie in the terahertz band [9]–[14]. In a study to probe the hybridization of nucleic acids and analyze a large number of genes simultaneously, Nagel et. al. have used integrated THz technologies [15], [16]. Youshida *et al.* have reported a THz biological sensor based on resonant transmission phenomena with the ability to detect small amounts of proteins [17]. In recent years, plasmonic metamaterial structures have been widely explored for sensing the refractive index of a substance at terahertz frequencies [18]–[22]. Metamaterials are artificially designed structures of

subwavelength dimensions and can exhibit plasmonic response for incoming terahertz radiations through careful design of its constituents. The properties of terahertz surface plasmon waves can be tailored based upon their constituent parameters [23]–[26]. Strategically designed plasmonic metamaterials are found to exhibit highly confined terahertz surface plasmon modes at the surface of the corrugated patterns which are very sensitive to minor environment changes [27].

THz sensing using plasmonic metamaterial structures can be performed either in transmission, reflection or waveguide configuration. In the reflection and transmission configurations, there is a little interaction of the analyte with the incident electromagnetic wave, which limits their sensing capability. However, in waveguide configuration, the incident wave, once coupled to the waveguide structure, interacts with the analyte that is attached to the constituent structures for several order of wavelengths. Several waveguide geometries have been investigated for their sensing capability in the last one decade [28]–[32]. In this context, Ma *et al.* have reported highly sensitive refractive index sensing of liquids by measuring a frequency shift in the waveguide transmission spectrum of the terahertz surface plasmons [33]. In this study, resonant plasmonic frequencies are shown to be strongly dependent on the refractive indices and thicknesses of analytes attached to the planar waveguide. They have successfully identified granular analytes of different quantities by measuring shifts in the resonant dips. In another study, Hanham *et al.* designed and fabricated a metal corrugated surface comprising of a linear array of subwavelength grooves [34], and investigated resonance shift of the fundamental mode by filling grooves with various fluids. Highly confined terahertz surface plasmons enhance the light-matter interactions and hence the sensitivity to identify an analyte located in the vicinity. You *et al.* have also reported a hybrid terahertz plasmonic waveguide for sensing an analyte by measuring a shift in the resonance dip with respect to the analytes of different quantities [35]. Recently, Islam *et al.* reported a comparative study of the sensing ability of a plasmonic waveguides with different shaped structures [36]. The sensitivity and figure of merit of the fundamental mode are compared for the rectangular and V-shaped grooves.

All the above cited schemes of terahertz sensing using plasmonic metamaterials are significant to perform label free refractive index sensing of an analyte and have focused upon fundamental mode excitation for the same. However, plasmonic waveguides also result in higher order modes depending upon the shape and size of its structures, which can be crucial for sensing analytes. Further, the role of high quality factor modes is important to sensing a substance, which has not been looked upon in plasmonic waveguides designed for sensor applications to the best of our knowledge. The excitation of high quality factor modes can results in highly sensitive detection with greater resolution. In this paper, we have tried to address these issues by designing a plasmonic waveguide capable of supporting multiple resonances. The fundamental and higher-order resonances are compared in terms of their Q-factor so as to have check on the quality of the modes and further to establish their sensing potential. The higher-order mode in plasmonic waveguides could be very significant in developing the highly sensitive refractive index sensors because of the high-quality factor as shown in our manuscript. The waveguide with pyramidal corrugations could be very advantageous in sensing analytes with better sensitivity because of its ability to strongly confine the electric field of the mode as well as filling the analyte quantity more effectively owing to its shape. The strong confinement to the surface is highly desirable for sensing applications as the analyte at the surface extensively interacts with the surface wave on the order of several wavelengths. As compared to previous investigations of sensing capabilities of plasmonic waveguide reported in the literature [32], [36], [37], we have observed that our design promises higher sensitivity for the 2^{nd} order mode compared to the fundamental mode.

In this paper, we study the sensing capability of a planar plasmonic terahertz waveguide consisting of an array of pyramidal grooves in one dimension. First, we numerically calculated the dispersion properties of the proposed plasmonic waveguide and examine frequency-domain THz waveguide transmission response for different groove lengths. The contour and color plot is analysed to present a comprehensive picture of the change of resonant behaviour with the change in length of grooves. We have also examined the dispersion properties of the waveguide with grooves of different heights in this section. In order to understand numerical observations, in the next section, we present an equivalent semi-analytical transmission line model and calculate

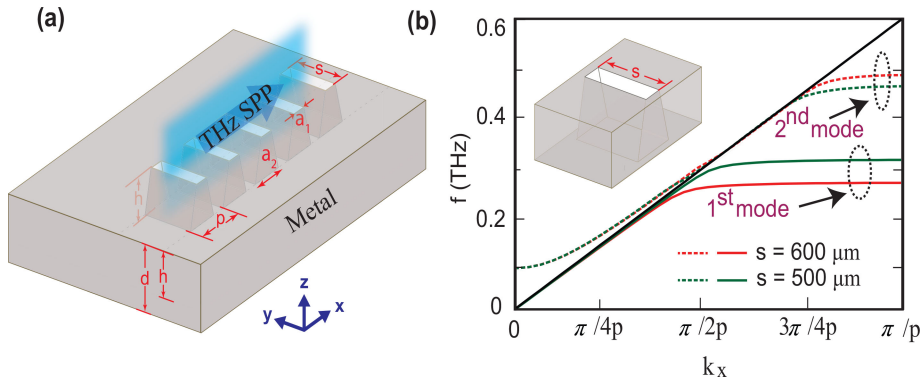

Fig. 1. (a) Waveguide Schematic: 3-Dimensional view of the waveguide comprising one dimensional array of periodic corrugations; (b) Numerically calculated dispersion properties of the fundamental and higher order modes in the proposed plasmonic waveguide having different transverse length of the pyramidal grooves i.e. $s = 600\ \mu m$ and $s = 500\ \mu m$.

the resonance response of waveguide in conjunction with the numerically obtained results for different groove lengths. In order to check the quality of the modes, we examine the quality factors of fundamental and higher-order modes in the next section. Further, we investigate the sensing capability of the modes by filling them with a fixed amount of analyte of different refractive indices while measuring their corresponding frequency shifts. In the end we provide a conclusion to our findings.

2. Waveguide Schematic and Dispersion Relations

The design of plasmonic waveguide and prior information of its constituent dimensions are crucial before proceeding to a complex fabrication process. In our study, we design one-dimensional plasmonic waveguide using periodically arranged subwavelength scale corrugations in the form of pyramidal grooves in a thin sheet of metal. The schematic of the proposed plasmonic waveguide geometry is shown in Fig. 1(a). The grooves parameters are chosen to be, length (s) = 0.5 mm, depth (d) = 0.5 mm, and periodicity (p) = 0.25 mm remain fix throughout the study. The grooves are pyramidal in shape with a narrow gap at the top. The upper and lower widths of the groves are chosen to be $a_1 = 0.05$ mm and $a_2 = 0.15$ mm respectively. The length of the grooves is varied for calculating dispersion relations and the terahertz waveguide transmission. The numerical simulations have been performed using the finite element time domain and the Eigen mode solver of the CST Microwave Studio simulation software. The waveguide structures are simulated under the open boundary condition in the x-y plane and periodic along the direction of light propagation. To ensure the plasmonic response of the proposed waveguide with different lengths of the pyramidal grooves, we have numerically examined dispersion relations of fundamental and higher-order modes without any analyte. We used the technique of finite element Eigen-mode solver for calculating dispersion relations under the periodic boundary conditions along the direction of propagation and absorbing layers along the transverse direction. We have assumed metal to be a perfect electrical conductor (PEC) owing to its high conductivity at terahertz frequencies. The results of the dispersion relations for two different lengths of the grooves are shown in Fig. 1(b). The dispersion relations of fundamental mode for $s = 600\ \mu m$ and $s = 500\ \mu m$ are represented by solid red and green traces, respectively, however the 2^{nd} order mode dispersion properties are represented by dotted blue and orange traces, respectively. The black line indicates the light line. From the plots, it may be noticed that the frequency monotonically increases in the beginning with the wavenumber, however it saturates at the boundary of 1^{st} Brillouin zone. As the length of the grooves is increased, the dispersion curves get red-shifted and saturates to a lower value.

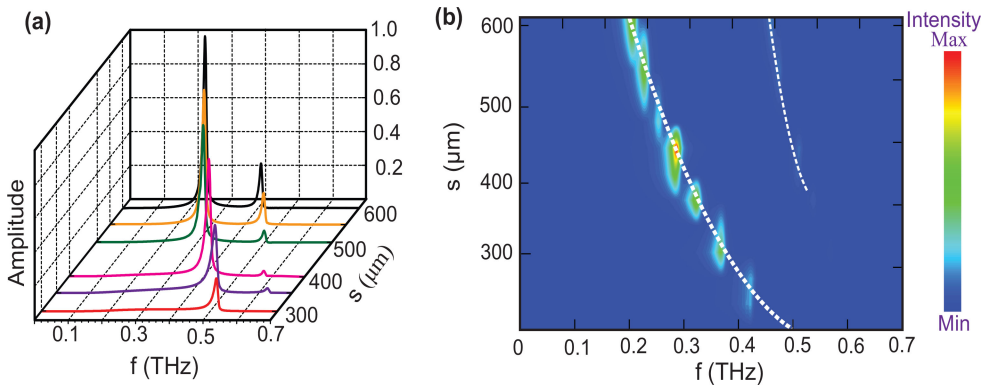

Fig. 2. (a) Numerically simulated frequency domain terahertz waveguide transmission for the plasmonic waveguides having pyramidal structure with different groove length i.e. $s = 600\ \mu m$, $550\ \mu m$, $500\ \mu m$, $450\ \mu m$, $400\ \mu m$, $350\ \mu m$, and $300\ \mu m$; (b) Contour plot of numerically simulated THz transmittance for different values of s.

3. THz Waveguide Transmission

In our numerical study, we excite the waveguide with a discrete source of single-cycle terahertz waveform at its one end. We assume a 4 cm long waveguide in our numerical simulations. The signal once coupled to the corrugated structures, it propagates along with one-dimensional waveguide pattern and finally detected at the other end. The detected time-domain signal is converted into the frequency domain spectra using Fast Fourier Transform (FFT). It is important to highlight that the proposed waveguide can be fabricated via conventional photolithography technique by using a highly doped silicon substrate while taking advantage of its crystalline structure. It is important to highlight that the proposed waveguide can be fabricated via conventional photolithography technique by using a highly doped silicon substrate while taking advantage of its crystalline structure. The corrugations of the waveguide depend on the crystal orientation of the silicon substrate. To make pyramidal grooves, one can use a crystalline silicon wafer of (100) orientation with dopant concentration, $n \geq 10^{19} cm^{-3}$ which behaves like a perfect conductor at terahertz frequencies. Using low-pressure chemical vapor deposition (LPCVD) technique, the silicon dioxide layer can be grown on the silicon surface and further, patterns can be made via photolithography technique [38], [39]. In the next step, appropriately patterned silicon can be etched in a mixture of potassium hydroxide, water, and isopropanol in the ratio of 60:30:10 to make inverted pyramidal apertures [40]. For the fabrication of groove, a silicon wafer can be glued on the back of the pyramidal apertures using a conducting epoxy. For characterization, one can use the technique of terahertz time-domain spectroscopy (THz-TDS) [41]. We have first calculated terahertz waveguide transmission for different lengths of the pyramidal structures. The results are shown in Fig. 2(a) the black traces represent terahertz frequency domain spectra for the case of $s = 600\ \mu m$. It is apparent from the spectra that it exhibits two resonant modes with anti-resonance frequencies of fundamental and 2^{nd} order mode appearing at 0.27 THz and 0.47 THz, respectively. The anti-resonance frequencies result from the interference of discrete and continuum spectrums and significant to terahertz waveguide transmission. As the length of the grooves is decreased, the anti-resonant frequencies of the modes get blue shifted. For $s = 500\ \mu m$, the frequencies of the fundamental and 2^{nd} order modes turns out to be 0.31 THz and 0.49 THz respectively. In our study, we have varied groove lengths as, $s = 600\ \mu m$, $500\ \mu m$, $400\ \mu m$, and $300\ \mu m$ and a blue shift trend in the anti-resonance frequencies is apparent from the figure. In order to present a comprehensive picture of this variation, in Fig. 2(b) we have shown the contour and color plot of the terahertz waveguide transmission. The decrease in groove length (s) causes the transmission curve to blue shift and saturate it to a higher anti-resonance frequency. A blue shift in the resonant behavior of the fundamental and 2^{nd} order mode is apparent. Further, we observe a decrease in

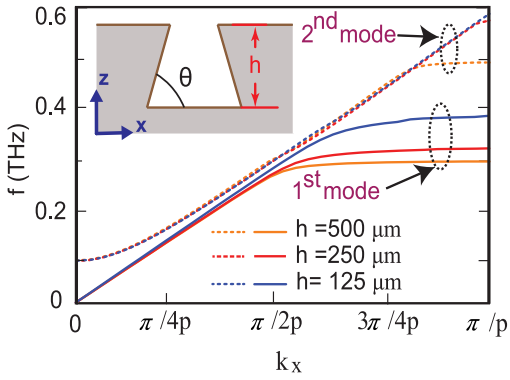

Fig. 3. Numerically calculated dispersion properties of fundamental and 2^{nd} order mode in pyramidal structured waveguide with three different depth grooves i.e. $h = 500\ \mu m$, $h/2 = 250\ \mu m$, $h/4 = 125\ \mu m$.

the amplitude of the resonances with the decrease in the groove width. This happens due to the lower field trapping capability of the smaller groove lengths. As we decrease the groove length to $s = 300\ \mu m$, we observe only the fundamental resonance, however 2^{nd} order modes completely vanish. From the contour figure it is clear that confinement of the electric field is changing with the length of the pyramidal grooves. In Fig. 2(b), the first trace is showing the fundamental mode and the second trace is showing the higher order mode. For the higher order mode, on decreasing the value of the groove length (s) electric field confinement is also reducing.

To examine the effect of depth of the grooves on terahetz wave propagation, we have calculated the dispersion relation of fundamental and higher order modes without any analyte from the finite element method for different depth of the grooves. Fig. 3 shows dispersion curves for three different depth of grooves (h) that is related to the slanted angle (θ) as $\theta = tan^{-1}(\frac{h}{a_2/2})$. For this study we have varied the groove depth from $h = 500\ \mu m$, $h/2 = 250\ \mu m$, $h/4 = 125\ \mu m$ and fixed other parameters of the structure at $a_1 = 50\ \mu m$, $a_2 = 220\ \mu m$ & $s = 500\ \mu m$. The dispersion relation of fundamental mode for $h = 500\ \mu m$, $h = 250\ \mu m$, and $h = 125\ \mu m$ are represented by solid orange, red, and blue traces respectively whereas dotted traces indicates the 2^{nd} order mode for the same. We note that as the depth of pyramidal grooves decreased, the dispersion curve saturates at higher frequency value.

4. Semi-Analytical Approach for Terahertz Transmission

In order to validate numerical finding and develop more physical insight into transmission response of the proposed plasmonic waveguide, we employ an equivalent semi-analytical transmission line model. The details of this approach in the context of plasmonic structures can be followed from the reference [42]. In the semi-analytical, the pyramidal groove in the metal sheet is assumed to be behaving like an RLC circuit under the transmission line approximation.

The circuit model of a unit cell is represented by two RLC circuits, where R_1, L_1, and C_1 correspond to the 1^{st} resonance and R_2, L_2, and C_2 correspond to the 2^{nd} resonance. These two resonances are coupled through the mutual inductance M. The circuit model of a unit cell under the transmission line theory is shown in Fig. 4. The intrinsic impedance (Z_0) of this circuit can be given as

$$Z_0 = \frac{120\pi}{\sqrt{\varepsilon_i}\left[\frac{w}{d} + 1.393 + 0.667 ln\left(\frac{w}{d} + 1.444\right)\right]} \tag{1}$$

The impedance of this circuit model Z_s can be written as

$$Z_s = \frac{Z_1 Z_2 + \omega^2 M^2}{[Z_1 + Z_2 - 2j\omega M]} \tag{2}$$

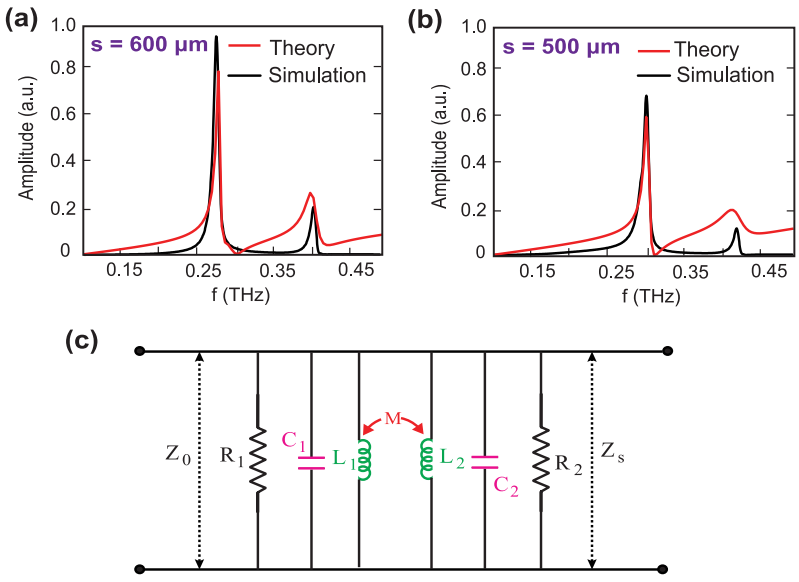

Fig. 4. (a) Waveguide transmission from transmission line theory(TL) for groove length $s = 600\ \mu$; (b) Waveguide transmission from transmission line theory (TL) for groove length $s = 500\ \mu m$; (c) Schematic of TL-RLC circuit model. The circuit components R_1, L_1, C_1 represents the resistance, inductance and capacitance related to 1st order resonance and R_2, L_2, C_2 represents the same related to higher order resonance. M is the mutual inductance responsible for coupling between resonance. Z_1 and Z_2 are impedances due to two circuits respectively. Whereas Z_0 and Z_s represent the impedances of free space and silicon substrate respectively.

TABLE I
Different Parameters Used in TL-RLC Circuit for Pyramidal Corrugation

Parameters	s=600 μm	s=500 μm
Resistance,R_1 (Ω)	4.0	2.9
Inductance, L_1 (fH)	60.5	38.1
Capacitance, C_1 (pF)	5.8	5.65
Resistance,R_2 (Ω)	0.5	0.3
Inductance, L_2 (fH)	12.0	9.9
Capacitance, C_2 (pF)	15.5	11.0

Where ω and M represents angular frequency and mutual inductance respectively. Z_1 and Z_2 correspond to the impedances due to 1st and 2nd LC circuits respectively. These impedances can be given as

$$Z_1 = \frac{L_1/C_1}{j\left(\omega L_1 - \frac{1}{\omega C_1}\right)}, Z_2 = \frac{L_2/C_2}{j\left(\omega L_2 - \frac{1}{\omega C_2}\right)} \tag{3}$$

The normalized transmission coefficient $t(\omega)$, of this transmission line-RLC circuit model will follow the normal form as

$$t(\omega) = \frac{2Z_s}{Z_0 + Z_s} \tag{4}$$

Where Z_0 and Z_s are the impedances of the substrate and free space, respectively. We have used Eq.(4) to calculate the waveguide transmission and predict anti-resonance frequencies of resonant modes. Using this model, we calculated terahertz transmission for the case of $s = 600$ μm, 500 μm and predicted that the anti-resonance frequencies matches with numerical findings for certain specific values of inductance, capacitance and resistance, which are given in Table 1. The values of R, L, C, and M are obtained by fitting the transmission amplitude with the simulations.

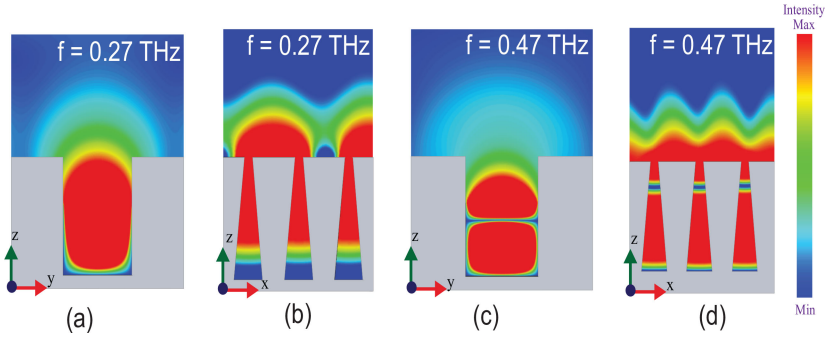

Fig. 5. The field profiles of the pyramidal structured plasmonic waveguide for different THz modes i.e. (a) Fundamental mode in zy -plane; (b) Fundamental mode in zx-plane plane. It represents electric field profile in the pyramidal groove at resonance frequency 0.27 THz; (c) 2^{nd} mode in zy-plane; (d) 2^{nd} mode in zx-plane It represents electric field profile in the pyramidal groove at resonance frequency 0.47 THz.

Here mutual inductance value is 96 *fH* and turns out to be fixed, indicating that coupling between two consecutive grooves is the same.

Further, we examine the field profiles of the terahertz modes supported by the proposed pyramidal structured plasmonic THz waveguide configuration. The results are shown in Fig. 5 for two different planes i.e. zy-plane and xy-plane. Fig. 5(a b) represent the field profile at the resonant frequencies of the fundamental mode i.e. 0.27 THz in zy-plane and xy-plane respectively, however Fig. 5(c d) represents the field profile of the 2^{nd} mode at 0.47 THz in the same plane. The structure exhibits strong confinement of all modes as it propagates along the waveguide. Fields are strongly confined at the resonant frequency and behaviour of the modes are apparent from the profile of modes.

5. Quality Factor and Sensor Characteristics of the Modes

Next, we examine the quality factor(Q) of the fundamental and higher-order modes of the proposed plasmonic waveguide. The quality factor is one of the very important parameters to analyse the quality of the modes and the narrowness of the resonance. The high Q-factor modes along with strong electric field confinement could be significant in the ultrasensitive sensing applications. The quality factor of a mode is defined as the ratio of resonance frequency (f_r) and its band width (Δf). The band width is basically the full width at half maxima of the resonance. We have calculated the quality factor for the fundamental and high order resonance of our waveguide for different transverse lengths (s) of the pyramidal grooves. The results have been shown in Fig. 6. The red trace shows the quality factor for the fundamental mode, however blue trace represents for 2^{nd} order mode. It may be noted that the quality factor (Q) of the fundamental mode decreases as the length of pyramidal grooves is increased. For $s = 300\ \mu m$, the Q-value is calculated to be 47.6, however it decreases to 33.8 as the length of the groove is increased to $s = 600\ \mu m$. A similar trend is observed in the case of 2^{nd} order mode. For 2^{nd} order mode, as the length of the groove is increased from $s = 400\ \mu m$ to $s = 600\ \mu m$, the quality factor is decreases 120.4 to 95.2 value. Our numerical observations also reveal that the Q-value of the 2^{nd} order mode is higher as compared to the fundamental mode owing to its narrow line width.

In order to examine the refractive index sensing capability of the modes in the proposed plasmonic waveguide, we filled pyramidal grooves with the analytes of different refractive indices. We measured the frequency shift of the fundamental as well as 2^{nd} order mode with respect to the change in refractive index of the analyte. Precisely, we focused on a change in the anti-resonant frequency of the mode when grooves are filled with analyte with respect to the intrinsic anti-resonant frequencies (i.e. without any analyte). For our study, we varied refractive index values

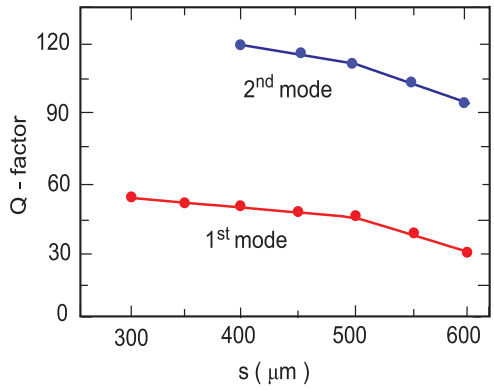

Fig. 6. Numerically calculated *Q*-factor of the Fundamental mode and higher order modes of plasmonic waveguide having Pyramidal grooves.

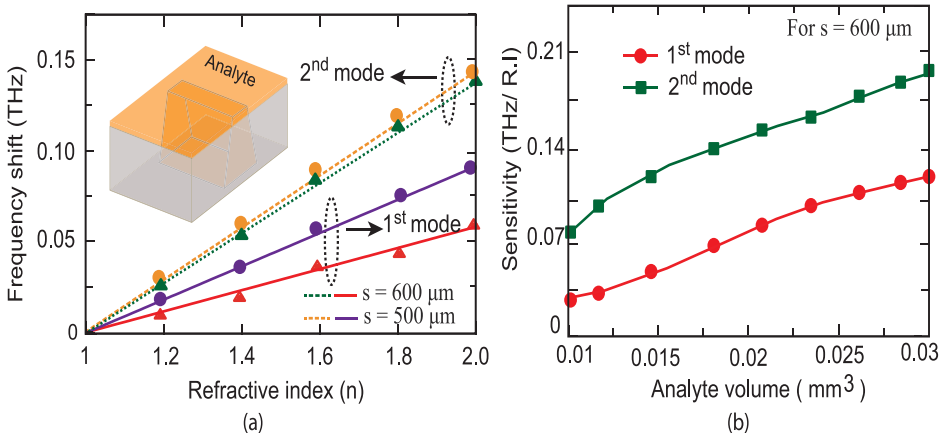

Fig. 7. (a) The variation of frequency shift of the fundamental mode higher order mode versus refractive index of the polyimide substance for the plasmonic terahertz waveguides. (b) Numerically calculated variation of sensitivity versus quantity of the analyte filling the pyramidal grooves.

of the analyte as $(n) = 1, 1.2, 1.4, 1.6, 2$. The results of frequency shift versus refractive index are shown in Fig. 7(a). When the refractive index of the analyte is increased, we observe a linear shift in the anti-resonance frequencies of the fundamental as well as 2^{nd} order mode. The shift in frequency is observed because of the interaction between the highly confined electric field of the modes at the surface and the analyte present there.

Further, we examine the sensitivity of the modes supported by our waveguide in order to comprehensively understand its sensing performance. The sensitivity is calculated by measuring frequency shift $((\Delta f))$with respect to the change in refractive index $((\Delta n))$ for a given amount of analyte, and calculating the slope $(\frac{\Delta f}{\Delta n})$ of this variation. Fig. 7(b) shows the plot of sensitivity of the modes versus volume of analyte filled in the grooves. We have varied refractive index as $(n) = 1, 1.2, 1.4, 1.6, 2.0$ to calculate correspond frequency shift for several different volumes of analytes for groove length $(s) = 600\ \mu m$. From the results, it is clear that sensitivity increases with the analyte quantity and this follows for fundamental as well as higher order modes. It may be observed from the plot that the 2^{nd} order mode results in higher sensitivity compared to the lower order mode. For 0.03 mm^3 of the analyte, the sensitivity for 2^{nd} modes is calculated to be $\frac{\Delta f}{\Delta n} = 0.19$ THz/RIU, whereas for the same quantity of analyte, the sensitivity of 1^{st} order modes turns out to be 0.11 THz/RIU.

6. Conclusion

In summary of this work, we have examined the sensing capability of a planar plasmonic terahertz waveguide comprising of subwavelength scale pyramidal shaped structures. We first examined dispersion relations of the fundamental and higher-order modes to ensure the plasmonic response of the proposed waveguide. The transmission response of the waveguide is examined for different transverse lengths of the corrugations. We observed that as the length of grooves is increased, the anti-resonant frequency of the fundamental and higher-order modes get red-shifted. We have further calculated the quality factors of the modes and examined their dependence on the transverse length of the structures. The quality factor decreases as the length is increased. For the same set of parameters, the quality factor is observed to be higher for 2^{nd} order mode compared to the fundamental mode. The high *Q*-factor modes are important to build highly sensitive refractive index sensors. The sensing capability of the fundamental and higher order modes is examined and compared by filling groves with materials of different refractive indices. As the refractive index of the analytes is increased, the resonances are found to be red-shifted. For a fixed value of analyte and groove parameters, the shift is higher for 2^{nd} mode compare to the 1^{st} mode. We further calculate the sensitivity of the modes for varying quantity of analyte. It is observed that the 2^{nd} order mode results in higher sensitivity compared to the lower order mode. For 0.03 mm^3 of the analyte, the sensitivity for 2^{nd} modes is calculated to be 0.19 THz/RIU, however for the same amount of analyte, it turns out to be 0.11 THz/RIU for the 1^{st} order mode. The present study not only compares the different modes ability to sense analyte, but also depicts better sensing capability than the earlier demonstrate transmission and waveguide approaches. The study could be significant in the construction of sensors and selectively choosing a guided wave mode to achieve high sensitivity in thin film refractive index terahertz sensors.

References

[1] M. Tonouchi, "Cutting-edge terahertz technology," *Nat. Photon.*, vol. 1, no. 2, pp. 97–105, Feb. 2007.
[2] X. C. Zhang and X. Jingzhou, "Introduction to THz wave photonics," vol. 29, New York, NY, USA: Springer, 2010.
[3] T. Nagatsuma, D. Guillaume, and C. R. Cyril, "Advances in terahertz communications accelerated by photonics," *Nat. Photon.*, vol. 10, no. 6, pp. 371–379, May 2016.
[4] X. C. Zhang, S. Alexander, and Z. Yan, "Extreme terahertz science," *Nat. Photon.*, vol. 11, no. 1, pp. 16–18, Jan. 2017.
[5] T. Kleine-Ostmann and N. Tadao, "A review on terahertz communications research," *J. Infrared, Millimeter, Terahertz Waves*, vol. 32, no. 2, pp. 143–171, Jan. 2011.
[6] D. Mittleman, ed., *Sensing With Terahertz Radiation*, vol. 85, Springer, Jan. 2013.
[7] D. Saeedkia, *Handbook of Terahertz Technology for Imaging, Sensing and Communications,* 1st Ed., Elsevier, 2013.
[8] Ho-Jin Song, and N. Tadao, "Present and future of terahertz communications," *IEEE Trans. Terahertz Sci. Technol.*, vol. 1, no. 1, pp. 256–263, Sep. 2011.
[9] J. Qin, X. Lijuan, and Y. Yibin, "Determination of tetracycline hydrochloride by terahertz spectroscopy with PLSR model," *Food Chem.*, vol. 170, pp. 415–422, Mar. 2015.
[10] K. Kawase *et al.*, "Non-destructive terahertz imaging of illicit drugs using spectral fingerprints," *Opt. Express*, vol. 11, no. 20, pp. 2549–2554, Apr. 2003.
[11] M. Walther *et al.*, "Chemical sensing and imaging with pulsed terahertz radiation," *Analytical Bioanalytical Chem.*, vol. 397, no. 3, pp. 1009–1017, Apr. 2010.
[12] J. Qin, X. Lijuan, and Y. Yibin, "Feasibility of terahertz time-domain spectroscopy to detect tetracyclines hydrochloride in infant milk powder," *Analytical Chem.*, vol. 86, no. 23, pp. 11750–11757, Oct. 2014.
[13] P. H. Bolivar *et al.*, "Label-free probing of genes by time-domain terahertz sensing," *Phys. Med. Biol.*, vol. 47, no. 21, Oct. 2002, Art. no. 3815.
[14] T. W. Crowe *et al.*, "Terahertz sources and detectors and their application to biological sensing," *Philosoph. Trans. Roy. Soc. London. Series A: Math., Phys. Eng. Sci.*, vol. 362, no. 1815, pp. 365–377, Dec. 2003.
[15] M. Nagel, M. Frst, and H. Kurz, "THz biosensing devices: Fundamentals and technology," *J. Phys.: Condensed Matter*, vol. 18, no. 18, pp. S601–S618, 2006.
[16] M. Nagel *et al.*, "Integrated THz technology for label-free genetic diagnostics," *Appl. Phys. Lett.*, vol. 80, no. 1, pp. 154–156, Jan. 2002.
[17] H. Yoshida *et al.*, "Terahertz sensing method for protein detection using a thin metallic mesh," *Appl. Phys. Lett.*, vol. 91, no. 25, Dec. 2007, Art. no. 253901.
[18] B. Ferguson and X. C. Zhang, "Materials for terahertz science and technology," *Nat. Materials*, vol. 1, no. 1, pp. 26–33, Sep. 2002.
[19] A. V. Zayats and M. Stefan, Eds., "Active plasmonics and tuneable plasmonic metamaterials," vol. 8. Wiley, 2013.
[20] S. Li, G. Kumar, and T. E. Murphy, "Terahertz nonlinear conduction and absorption saturation in silicon waveguides," *Optica*, vol. 2, no. 6, pp. 553–557, 2015.

[21] G. Kumar *et al.*, "Terahertz surface plasmon waveguide based on a one-dimensional array of silicon pillars," *New J. Phys.*, vol. 15, no. 8, 2013, Art. no. 085031.
[22] X. Hu *et al.* "Metamaterial absorber integrated microfluidic terahertz sensors," *Laser Photon. Rev.*, vol. 10, no. 6, pp. 962–969, 2016.
[23] S. E. Irvine, A. Dechant, and A. Y. Elezzabi, "Generation of 0.4-keV femtosecond electron pulses using impulsively excited surface plasmons," *Phys. Rev. Lett.*, vol. 93, no. 18, 2004, Art. no. 184801.
[24] S. E. Irvine and A. Y. Elezzabi, "Surface-plasmon-based electron acceleration," *Phys. Rev. A*, vol. 73, no. 1, 2006, Art. no. 013815.
[25] M. Raynaud *et al.*, "Strongly enhanced laser absorption and electron acceleration via resonant excitation of surface plasma waves," *Phys. Plasmas*, vol. 14, no. 9, 2007, Art. no. 092702.
[26] S. Li *et al.*, "Terahertz surface plasmon polaritons on a semiconductor surface structured with periodic V-grooves," *Opt. Express*, vol. 21, no. 6, pp. 7041–7049, 2013.
[27] W. Xu, L. Xie, and Y. Ying, "Mechanisms and applications of terahertz metamaterial sensing: A review," *Nanoscale*, vol. 9, no. 37, pp. 13864–13878, 2017.
[28] S. Li *et al.*, "Plasmonic terahertz waveguide based on anisotropically etched silicon substrate," *IEEE Trans. Terahertz Sci. Technol.*, vol. 4, no. 4, pp. 454–458, Jul. 2014.
[29] Y. Yang *et al.*, "Terahertz topological photonics for on-chip communication," *Nat. Photon. 14*, pp. 446–451, 2020.
[30] Y. Ma, B. Dong, and C. Lee, "Progress of infrared guided-wave nanophotonic sensors and devices," *Nano Convergence*, vol. 7, no. 12, 2020.
[31] Z. Ren *et al.*, "Leveraging of MEMS technologies for optical metamaterials applications," *Adv. Opt. Mater.*, vol. 8, no. 3, 2020, Art. no. 1900653.
[32] B. Dong *et al.*, "Recent progress in nanoplasmonics-based integrated optical micro/nano-systems," *J. Phys. D: Appl. Phys.*, vol. 53, 2020, Art. no. 213001.
[33] Z. Ma *et al.*, "Terahertz particle-in-liquid sensing with spoof surface plasmon polariton waveguides," *APL Photon.*, vol. 2, no. 11, 2017, Art. no. 116102.
[34] S. M. Hanham *et al.*, "Exploiting plasmonics for THz and infrared sensing," *Terahertz Phys., Devices, Syst. VIII: Adv. Appl. Ind. Defense*, vol. 9102, International Society for Optics and Photonics, 2014.
[35] B. You *et al.*, "Hybrid terahertz plasmonic waveguide for sensing applications," *Opt. Express*, vol. 21, no. 18, pp. 21087–21096, 2013.
[36] I. Maidul *et al.*, "Terahertz plasmonic waveguide based thin film sensor," *J. Lightw. Technol.*, vol. 35, no. 23, pp. 5215–5221, 2017.
[37] L. Tian *et al.*, "Investigation of mechanism: Spoof SPPs on periodically textured metal surface with pyramidal grooves," *Sci. Reports*, vol. 6, 2016, Art. no. 32008.
[38] G. Kumar *et al.*, "Planar plasmonic terahertz waveguides based on periodically corrugated metal films," *New J. Phys.*, vol. 13, no. 3, 2011, Art. no. 033024.
[39] S. Li *et al.*, "Terahertz surface plasmon polaritons on a semiconductor surface structured with periodic V-grooves," *Opt. Express*, vol. 21, no. 6, pp. 7041–7049, 2013.
[40] S. Sriram and E. P. Supertzi, "Novel V-groove structures on silicon," *Appl. Opt.*, vol. 24, no. 12, pp. 1784–1787, 1985.
[41] G. Kumar *et al.*, "Terahertz surface plasmon waveguide based on a one-dimensional array of silicon pillars," *New J. Phys.*, vol. 15, no. 8, 2013, Art. no. 085031.
[42] D. M. Pozar, "Microwave engineering," John Wiley & Sons, 2009.